ELSEVIER

Chemical Geology 147 (1998) 233–248

CHEMICAL GEOLOGY
INCLUDING
ISOTOPE GEOSCIENCE

Diopside and anthophyllite dissolution at 25° and 90°C and acid pH

Yang Chen [1], Susan L. Brantley *

Dept. of Geosciences, Pennsylvania State University, University Park, PA 16802, USA

Received 17 February 1997; accepted 28 November 1997

Abstract

Dissolution experiments of diopside and anthophyllite were conducted in continuously stirred flow-through reactors at temperatures of 25° and 90°C at acid pH. Stoichiometric steady state was reached at ~2700 h (at 25°) or ~1000 h (90°C). Specific surface area significantly increased after dissolution of diopside but not anthophyllite. Extensive etch pits were observed on some of the reacted surfaces of diopside grains. The observed etch pits are preferentially developed along the exsolution lamellae boundaries between diopside and pigeonite or hypersthene. The surface morphology observed on our laboratory-leached samples is very similar to that observed on naturally weathered pyroxene grains by previous workers. No etch pits were observed on the surface of anthophyllite. Presumably, dissolution of anthophyllite results in the disintegration of fibrous anthophyllite without observable etching. Under the experimental conditions, dissolution rates of diopside and anthophyllite are pH-dependent, and the pH-dependence increases with increasing temperature. For diopside, the reaction order n with respect to H^+ increases from 0.19 ± 0.06 at 25°C to 0.76 ± 0.08 at 90°C, while for anthophyllite, the value of n increases from 0.24 ± 0.03 at 25°C to 0.63 ± 0.04 at 90°C. This result indicates that when temperature increases, the rate of increase in pH-dependence is faster for diopside than for anthophyllite. Activation energies (E_a) have been estimated for diopside and anthophyllite dissolution based on dissolution at the two temperatures. The values of pH-independent E_a are 22.8 ± 1.6 and 19.4 ± 0.9 kcal mol^{-1} for diopside and anthophyllite, respectively. Both of the activation energies are well above the E_a of transport in solution (5 kcal mol^{-1}), and significantly smaller than the E_a of breaking bonds in crystals.

Keywords: Diopside; Anthophyllite; Inosilicate; Dissolution; Kinetics; Experiment

1. Introduction

Because of instability under surface conditions, weathering of pyroxenes and amphiboles provides a major source of Mg, Fe and Ca in natural waters. Weathering of Ca, Mg-containing silicates is of particular importance because of the role of Ca and Mg cycling in controlling the long-term atmospheric CO_2 budget, and by implication, on the global climate. Despite the importance of the weathering of these minerals, relatively few studies have assessed the dissolution kinetics of these phases in the laboratory and in the field [for a summary, see the recent review by Brantley and Chen (1995)].

* Corresponding author.
[1] L. Robert Kimball and Associates, 615 West Highland Ave., P.O. Box 1000, Ebensburg, PA 15931, USA.

0009-2541/98/$19.00
PII: S0009-2541(98)00016-3

Considerable discrepancies exist in the literature concerning the dissolution kinetics of inosilicates, and, particularly, the pH- and temperature-dependence of their dissolution rates (Luce et al., 1972; Schott et al., 1981; Rimstidt and Dove, 1986; Ferruzzi, 1993; Knauss et al., 1993; Xie, 1994). Two of the sources of these discrepancies may be differences in types of chemical reactors used for dissolution studies and differences in experimental duration. A continuously stirred tank reactor (CSTR) has a major advantage over a batch reactor in that a CSTR can assess the dissolution kinetics under constant solution chemistry (Hill, 1977). However, the duration of reaction with a CSTR must be long enough for the system to reach the steady state condition, where the rate of dissolution is constant. This usually means that several thousand hours are needed in order to get a single rate measurement for inosilicate dissolution under ambient temperatures [e.g., for hornblende, see the work of Zhang et al. (1993)]. Reaction durations vary from worker to worker [e.g., for wollastonite, < 20 h, see the work of Rimstidt and Dove (1986); 500 h, see the work of Xie (1994)], and it is reasonable to assume that the results obtained for very short durations may not have reached true steady state.

Another source of discrepancy is the choice of normalization factor for the measured dissolution flux. Several authors reported dissolution rates of inosilicates normalized to the initial surface area as measured by BET adsorption isotherm (Knauss et al., 1993; Xie, 1994). This approach may differ from normalization by final surface area since the specific surface area often changes through dissolution. A doubling in surface area may result in an error of 0.3 log units to the rate. In addition, some authors reported the dissolution rates normalized to the mass or assumed surface area estimated from the geometry of the starting materials (Schott et al., 1981; Siegel and Pfannkuch, 1984). The surface area of inosilicates measured by BET commonly differs from the geometric surface area by factors of 3 to 13 (Luce et al., 1972; Schott and Berner, 1983; Rimstidt and Dove, 1986; Mast and Drever, 1987; Knauss et al., 1993; Xie and Walther, 1994; Banfield et al., 1995).

However, a controversy exists as to whether the initial or final BET surface area is appropriate to use. Data reported by Murphy and Drever (1993) and Drever et al. (1994) suggest that the initial BET area is the appropriate number, whereas Stillings and Brantley (1995) observed the opposite in their investigation of feldspar dissolution.

Another important but often unnoticed error occurs when experiments are run close to neutral pH. Evaluation of data reported in the literature shows that many near-neutral solutions used in inosilicate dissolution experiments were supersaturated with respect to one or more secondary phases [e.g., diopside dissolution by Schott et al. (1981); augite dissolution by Siegel and Pfannkuch (1984); hornblende dissolution by Zhang et al. (1993)]. Supersaturation of secondary phases may correlate with slow dissolution of the primary phase due to lowered chemical affinity, precipitation of armoring phases, or difficult data interpretation.

Some workers used buffer solutions in their experiments in order to maintain constant pH and ionic strength [e.g., for diopside dissolution by Schott et al. (1981) and Knauss et al. (1993); for enstatite dissolution by Schott et al. (1981)]. However, as indicated by several workers, use of buffers may have side effects on dissolution kinetics of silicate minerals due to the formation of complexes which may accelerate or inhibit the dissolution of the phase of interest (Dove and Crerar, 1990).

The proton-promoted dissolution rate, r, at low pH is usually expressed as:

$$r = k[H^+]^n \quad (1)$$

or

$$\log r = \log k - n\,\mathrm{pH} \quad (2)$$

where k is the apparent rate constant, n is the apparent reaction order with respect to H^+, and $[H^+]$ refers to H^+ activity. Both k and n are temperature-dependent (Laidler, 1987; Brady and Walther, 1992; Casey and Sposito, 1992). Because of the different approaches used in obtaining dissolution rate data, the reported pH-dependence of dissolution for pyroxenes and amphiboles varies from worker to worker. For the pyroxene group, values of n as high as 0.7 (Schott et al., 1981; Schott and Berner, 1985) or as low as 0.2 (Knauss et al., 1993) have been reported for diopside at room temperatures. Similar discrepancies also exist for enstatite: the reported values of n at room temperature range from 0 to 0.8 (Luce et al., 1972; Schott et al., 1981; Schott and Berner, 1985;

Ferruzzi, 1993). Dissolution data for the amphibole group are rare in the literature; however, values ranging from 0 [anthophyllite, see the work of Mast and Drever (1987)] to 0.7 [hornblende, see the works of Zhang et al. (1993) and Sverdrup (1990)] were reported at room temperature.

The literature data also show great variation in activation energy (E_a) of inosilicate dissolution. For example, values of E_a ranging from 9 to 36 kcal mol^{-1} (Sanemasa and Kataura, 1973; Schott et al., 1981; Schott and Petit, 1987; Knauss et al., 1993) were reported for diopside dissolution. No E_a data are available in the literature for amphibole dissolution.

The surface protonation model (Schindler, 1981; Stumm and Furrer, 1987; Blum and Lasaga, 1988, 1991; Brady and Walther, 1989) is the most commonly used model in describing the dissolution kinetics of oxides and silicates. According to this model, the surface hydroxyl groups are protonated or deprotonated with variation in pH. The pH_{pznpc} is defined for each mineral as the pH in which the concentration of positively charged surface sites equals the concentration of negatively charged surface sites in the absence of specifically adsorbed cations or anions. According to the surface protonation model, the dissolution rate of the mineral is dependent on the concentration of the protonated surface sites at $pH < pH_{pznpc}$. Results of proton adsorption experiments show that proton adsorption enthalpies are consistently exothermic and that the pH_{pznpc} decreases as temperature increases (Machesky, 1989; Brady and Walther, 1992). This observation led Brady and Walther (1992) to suggest that as temperature increases, the absolute value of n will increase.

According to Casey and Sposito (1992), at $pH < pH_{pznpc}$, the E_a for proton-promoted dissolution can be separated into three terms: the activation enthalpy of dissolution, the enthalpy of proton adsorption, and the enthalpy that arises from long-range electrostatic interactions among charged surface groups. They proposed that the last term would introduce a significant pH-dependence in the experimental E_a. In other words, their model, in agreement with that of Brady and Walther (1992), predicts that as temperature increases, dissolution rate will become more pH-dependent (n will increase).

Literature data on the temperature effect of pH-dependence of inosilicate dissolution do not agree. For example, Schott et al. (1981) and Schott and Berner (1985) reported that for diopside dissolution in acid solutions, the value of n increased from 0.7 to 0.75 when temperature increased from 20° to 50°C, whereas Knauss et al. (1993) reported a constant value of 0.2 at temperatures from 25° to 90°C. For double-chain silicates, no data are reported in the literature.

The goal of this study was to determine the dissolution kinetics of diopside and anthophyllite under well constrained conditions. To overcome the problems discussed earlier in this section, we ran the dissolution experiments of inosilicates in dilute HCl solutions using continuously stirred flow-through reactors. The flow rates were so selected that the solutions were far from equilibrium with any of the possible solid phases listed in the database of SOLMINEQ (Kharaka et al., 1988). Also, we ran the experiments over long timescales (thousands of hours) to reach true steady states. The dissolution rates were normalized using the final BET surface area. Initial surface areas are also reported. Under these conditions, reliable data can be obtained concerning the pH- and temperature-dependence of the dissolution rates.

This study is a part of our work on dissolution kinetics of silicates with different structures. One of our purposes is to compare the dissolution data of pyroxenes and amphiboles with those of other silicates.

2. Materials and methods

2.1. Starting materials

Diopside and anthophyllite were obtained from Ward's Natural Science. The diopside samples, inaccurately named as enstatite in Ward's catalog, were from Kangan of Andhra-Pradish, India, while the anthophyllite samples derived from Rakabedo Mines of Udaipur, India. Bulk chemical analyses on cleaned (see below) samples, based on the lithium metaborate fusion method (Shapiro, 1975), are listed in Table 1. The mineralogies of the cleaned bulk samples were confirmed by X-ray diffraction. The diopside samples were also examined using electron mi-

Table 1
Mineral composition

	SiO_2	MgO	CaO	Fe_2O_3	Al_2O_3	Na_2O	TiO_2	MnO	P_2O_5
Bulk chemical analysis (lithium metaborate fusion)									
Diopside	54.20	14.70	19.40	7.43	2.42	0.63	0.22	0.13	0.09
Anthophyllite	59.50	29.00	0.40	9.64	0.42	0.02	0.02	0.02	0.12
Electron microprobe analysis									
Bulk diopside	50.47	12.82	21.70	7.46	4.36	1.15			
	50.07	12.90	21.23	7.26	4.56	1.23			
Lamellae in diopside sample	49.94	20.97	1.74	24.68	2.59	0.02			
	49.58	20.86	1.42	22.95	3.14	0.07			

Values are expressed as wt.% of oxide.
Mineral compositions based on bulk chemical analysis are: diopside: $Ca_{0.8}Mg_{0.8}Fe_{0.2}Al_{0.1}Si_2O_6$; anthophyllite: $Mg_{5.7}Fe_{1.0}Al_{0.1}Si_{7.8}O_{22}(OH)_2$.

croprobe for possible exsolution. On a few samples, we observed under back-scattered electron microscopy, lamellae of different composition. The composition of the lamellae is characterized by relatively low Ca and high Mg and Fe contents, similar to pigeonite or hypersthene. Results of the microprobe analysis are also listed in Table 1. We also observed occasional dolomite and rutile inclusions. Rutile was always seen in the lamellae. The inclusions were usually less than 10 μm in dimension.

Diopside samples were hammer-crushed, dry-ground using an agate mortar, and then sieved to obtain the size fraction of 100–200 mesh (150–75 μm). The powder sample was then ultrasonically cleaned of ultrafines in spectroscopic grade acetone and the supernatant was decanted. Ultrasonication was repeated several times until the decanted solution was clear.

The procedure of treatment for anthophyllite was different than that of diopside because of the fibrous nature of this mineral. Anthophyllite samples were first crushed using a hammer, and then put into a blender containing pure methanol. After about 30 min of treatment, the samples were dried at room temperatures and sieved to obtain the 35–400 mesh size fraction (corresponding to 500 to 38 μm). This sample was then ultrasonically cleaned in pure acetone. However, even after repeatedly cleaning the samples, we were unable to get clear supernatants, and we therefore used the samples after cleaning more than a dozen times.

Both mineral samples were dried in an oven at 105°C and stored in a desiccator before experiments.

2.2. Apparatus

Dissolution experiments were performed using continuously stirred flow-through reactors. Reactors of polycarbonate and Teflon were used for experiments at 25°C (Fig. 1A), and reactors made from titanium were used at 90°C (Fig. 1B). The details of the reactor design and flow system configurations were similar to those for albite dissolution experiments discussed in the work of Chen and Brantley

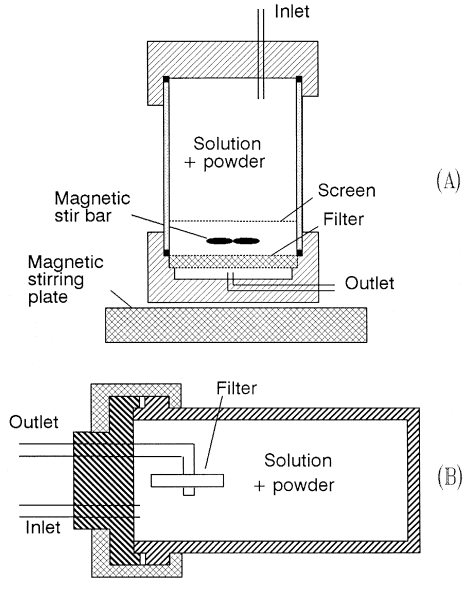

Fig. 1. Schematic diagram showing continuously stirred flow-through reactors. (A) Reactor made from polycarbonate, used for experiments at 25°C. (B) Reactor made from titanium (parts show in hachures), used for experiments at 90°C. The gasket was made of Teflon, and the filter was made of PTFE.

Table 2
Experimental conditions

RUN	T (°C)	pH		Flow rate (ml h^{-1})	Mass of sample (g)	Duration (h)
		inlet	outlet[a]			
Diop25-1	25	1.0	1.23	0.35 ± 0.003	2.00	3400
Diop25-2	25	2.0	2.05	0.35 ± 0.003	2.00	3400
Diop25-3	25	3.0	3.16	0.50 ± 0.01	2.00	3400
Diop25-4	25	3.5	3.55	0.52 ± 0.01	2.00	3400
Diop90-B	90	2.0	2.17	0.96 ± 0.02	2.00	1830
Diop90-C	90	3.0	3.18	1.92 ± 0.01	2.00	1830
Diop90-D	90	3.5	3.82	1.84 ± 0.03	2.00	1830
Anth25-1	25	1.0	1.24	0.36 ± 0.01	1.00	3400
Anth25-2	25	2.0	2.04	0.35 ± 0.004	1.00	3400
Anth25-3	25	3.0	3.12	0.48 ± 0.01	1.00	3400
Anth25-4	25	3.5	3.58	0.54 ± 0.07	1.00	3400
Anth90-A	90	1.0	1.09	0.82 ± 0.03	1.00	1380
Anth90-B	90	2.0	1.93	0.82 ± 0.11	1.00	1380
Anth90-C	90	3.0	2.99	1.91 ± 0.03	1.00	1380
Anth90-D	90	3.5	3.55	1.96 ± 0.01	1.00	1380

[a]Outlet pH at 90°C was corrected to 90°C by means of SOLMINEQ using the value measured at room temperature.

(1997). Reactors at 25°C were stirred by magnetic stir bars, while reactors at 90°C were continuously rotated back and forth.

2.3. Chemical analyses and surface area measurements

The pH values of all solutions were measured using an Orion 940 pH meter with an Orion Ross combination pH electrode at room temperature. The analytical uncertainty in pH measurement is ± 0.02. Effluent solutions, continuously collected and acidified with 1:10 HCl, were analyzed for Si, Mg, Ca, Fe, and Al with a PC3000 Leeman Labs ICP emission spectrometer and with a Spectronic 601 spectrophotom-eter (heteropoly blue method, see the work of Greenberg et al. (1985) for Si concentrations in solutions collected during anthophyllite dissolution at 25°C, and during diopside dissolution at pH 3.5 and 25°C, where concentrations were too low for ICP).

Values of pH of the solutions at 90°C were calculated from the values measured at 25°C using the computer code SOLMINEQ, Version 1988 (Kharaka et al., 1988). This code uses mass balance and mass action to calculate $[H^+]$. The calculated 90°C pH values are very close to those measured at room temperature with a maximum difference of 0.02 units. Specific surface areas of samples before and after experiments were measured using a three-point BET method with Kr as the adsorbate on a Quantasorb Sorption System QS-10 by Quantachrome.

2.4. Experimental conditions

Table 2 shows all the experimental conditions. The dissolution experiments were conducted at temperatures of 25° and 90°C and initial pH values from 1 to 3.5. All starting solutions were prepared with pure HCl and no buffer solution in order to avoid possible inhibition or promotion effects of foreign species. The pH values range from 1.23 to 3.55 for the effluent solutions. The flow rate differs from experiment to experiment (Table 2). For experiments at 90°C, the flow rates were 0.86 to 1.96 ml h^{-1}. For experiments run at 25°C, flow rates were doubled at $\sim$2000 h in order to attempt to speed the rate of attainment of steady state (faster flow rates cause slightly lower pH values because of lower residence times in the reactors). The flow rates listed in Table 2 were the final rates of the experiments.

2.5. Calculation of dissolution rates and Gibbs free energy of reaction

The release rates of Si, Ca, Mg, Fe and Al for diopside and anthophyllite dissolution were calculated using the following equation:

$$r_i = Q C_i / (3{,}600{,}000\, S v_i) \quad (3)$$

where r_i is the release rate of element i (mol cm^{-2} s^{-1}) normalized for mineral stoichiometry, Q is the volumetric flow rate (ml h^{-1}), C_i is the effluent concentration of i (mol l^{-1}), S is the final surface area (cm^2), and v_i is the stoichiometric coefficient of element i in the mineral formula. Rates were calculated from averages over the last few measurements when dissolution was at steady state, i.e., concentrations were nearly constant.

For both minerals, the Si concentration in solution was measured accurately by ICP and spectrophotometry methods throughout the dissolution experiments. However, measurement of the other elements was problematic, due to lower concentrations in some cases. Hence, in the subsequent discussions, the release or dissolution rates are all based on Si concentrations unless otherwise specified.

The error of measurement in dissolution rates is estimated based on errors in chemical analysis ($\pm 5\%$), flow rate (± 0.3–12%), and surface analysis ($\pm 25\%$).

Gibbs free energy of reaction (ΔG) is defined in the following equation:

$$\Delta G = RT \ln(Q/K_{eq}) \quad (4)$$

where R is the universal gas constant, T is temperature, Q represents the reaction activity quotient, and K_{eq} stands for the equilibrium constant of the dissolution reaction at the temperature and pressure of interest.

The computer code SOLMINEQ (Kharaka et al., 1988) was used to calculate the ΔG values. SOLMINEQ uses the iteration technique for the mass balance calculation and an extended Debye–Huckel equation for the activity coefficient model.

The thermodynamic data used to calculate the ΔG value of diopside in SOLMINEQ are taken from the works of Helgeson (1985) and Robie et al. (1978). Data for anthophyllite dissolution are from the work of Helgeson et al. (1978).

The ΔG values for both diopside and anthophyllite were calculated assuming congruent dissolution of the pure endmember of the corresponding phase:

$$\text{Diopside: } CaMgSi_2O_6 + 4H^+ + 2H_2O \Leftrightarrow Ca^{2+} + Mg^{2+} + 2H_4SiO_4^0 \quad (5)$$

$$\text{Anthophyllite: } Mg_7Si_8O_{22}(OH)_2 + 14H^+ + 8H_2O \Leftrightarrow 7Mg^{2+} + 8H_4SiO_4^0 \quad (6)$$

No attempt was made to estimate the ΔG for the exact composition of our diopside and anthophyllite samples (Table 1).

3. Results

Dissolution experiments were run for 3400 h at 25°C for both diopside and anthophyllite, but 1380 h and 1830 h at 90°C for anthophyllite dissolution and diopside dissolution, respectively.

The measured initial surface areas of diopside and anthophyllite samples were 860 and 12,100 cm^2 g^{-1}, respectively. Dissolution of diopside under all experimental conditions resulted in increased specific surface areas which range from 1300 to 2340 cm^2 g^{-1} (Table 3). The largest increase (factor of 2.7) was observed after dissolution at 90°C and pH 3.18 for 1830 h (Run Diop90-C). The change in specific surface area for anthophyllite after experiments was minimal: except for experiment Anth90-A (which decreased from 12,100 to 7610 cm^2 g^{-1}), little change in specific surface area was observed under any conditions (Table 4). Tables 3 and 4 show the results of our diopside and anthophyllite dissolution experiments at 25° and 90°C and at various pH conditions.

The concentrations and dissolution rates shown in Tables 3 and 4 are steady state values calculated when concentration and flow rate were constant. The Si-based rates vary from 4.3×10^{-16} to 7.7×10^{-14} mol cm^{-2} s^{-1} for diopside dissolution and from 4.9×10^{-18} to 3.1×10^{-15} mol cm^{-2} s^{-1} for anthophyllite under the different conditions. The dissolution rates calculated based on Ca and Mg concentrations for diopside and that based on Mg and Fe for anthophyllite are also listed in the tables.

The experimental results are also presented in terms of the time evolution of the normalized release rates of Si, Mg, Ca and Fe (if applicable) in Fig. 2a–d. Note that during the course of experiments for diopside and anthophyllite dissolution at 25°C, we doubled the flow rate. The change in flow rate is reflected by the discontinuity at about 2000 h shown in Fig. 2a and c.

Solubility calculations completed for experimental solutions show that the solutions were undersaturated with respect to any likely secondary phases. The ΔG values for diopside dissolution calculated based on

Table 3
Results of diopside dissolution experiments

RUN	T (°C)	pH[a]	Concentration (mol l^{-1})			ΔG	Final area[b]	Dissolution rate (mol cm^{-2} s^{-1})[c]		
			Si	Ca	Mg	(kcal mol^{-1})	(cm^2 g^{-1})	Based on Si (±error)	Based on Ca (±error)	Based on Mg (±error)
Diop25-1	25	1.23	1.08×10^{-4}	3.70×10^{-5}	3.87×10^{-5}	−44.0	1300	$2.0\times10^{-15}\pm5.2\times10^{-16}$	$1.7\times10^{-15}\pm4.4\times10^{-16}$	$1.8\times10^{-15}\pm4.6\times10^{-16}$
Diop25-2	25	2.05	8.78×10^{-5}	3.68×10^{-5}	4.24×10^{-5}	−38.8	1940	$1.1\times10^{-15}\pm2.8\times10^{-16}$	$1.2\times10^{-15}\pm2.9\times10^{-16}$	$1.3\times10^{-15}\pm3.4\times10^{-16}$
Diop25-3	25	3.16	4.65×10^{-5}	1.86×10^{-5}	1.82×10^{-5}	−34.2	1570	$1.0\times10^{-15}\pm2.6\times10^{-16}$	$1.0\times10^{-15}\pm2.6\times10^{-16}$	$1.0\times10^{-15}\pm2.6\times10^{-16}$
Diop25-4	25	3.55	2.19×10^{-5}	8.26×10^{-6}	6.57×10^{-6}	−34.0	1390	$5.7\times10^{-16}\pm1.5\times10^{-16}$	$5.4\times10^{-16}\pm1.4\times10^{-16}$	$4.3\times10^{-16}\pm1.1\times10^{-16}$
Diop90-B	90	2.16	1.02×10^{-5}	4.03×10^{-4}	4.83×10^{-4}	−32.6	880	$7.7\times10^{-16}\pm2.0\times10^{-16}$	$7.6\times10^{-14}\pm2.0\times10^{-14}$	$9.1\times10^{-14}\pm2.3\times10^{-14}$
Diop90-C	90	3.18	1.74×10^{-4}	7.28×10^{-5}	7.67×10^{-5}	−30.9	2340	$9.9\times10^{-15}\pm2.5\times10^{-15}$	$1.0\times10^{-14}\pm2.6\times10^{-15}$	$1.1\times10^{-14}\pm2.8\times10^{-15}$
Diop90-D	90	3.82	7.36×10^{-5}	3.19×10^{-5}	3.25×10^{-5}	−28.7	2180	$4.3\times10^{-15}\pm1.1\times10^{-15}$	$4.7\times10^{-15}\pm1.2\times10^{-15}$	$4.8\times10^{-15}\pm1.2\times10^{-15}$

[a]At experimental temperature.
[b]Initial specific surface area = 860 cm^2 g^{-1}.
[c]Rates are in mol diopside, using the composition listed in Table 1.

Table 4
Results of anthophyllite dissolution experiments

RUN	T (°C)	pH[a]	Concentration (mol l^{-1})			ΔG	Final area[b]	Dissolution rate (mol cm^{-2} s^{-1})[c]		
			Si	Mg	Fe	(kcal mol^{-1})	(cm^2 g^{-1})	Based on Si (±error)	Based on Mg (±error)	Based on Fe (±error)
Anth25-1	25	1.24	1.68×10^{-5}	1.84×10^{-5}	2.56×10^{-6}	−129.5	10,690	$2.0\times10^{-17}\pm5.2\times10^{-18}$	$3.0\times10^{-17}\pm7.7\times10^{-18}$	$2.4\times10^{-17}\pm6.1\times10^{-18}$
Anth25-2	25	2.04	1.05×10^{-5}	8.27×10^{-6}	1.70×10^{-6}	−119.7	12,790	$1.0\times10^{-17}\pm2.6\times10^{-18}$	$1.1\times10^{-17}\pm2.8\times10^{-18}$	$1.3\times10^{-17}\pm3.3\times10^{-18}$
Anth25-3	25	3.12	5.61×10^{-6}	2.97×10^{-6}	1.18×10^{-6}	−106.3	14,240	$6.7\times10^{-18}\pm1.7\times10^{-18}$	$4.9\times10^{-18}\pm1.2\times10^{-18}$	$1.1\times10^{-17}\pm2.8\times10^{-18}$
Anth25-4	25	3.56	3.36×10^{-6}	7.14×10^{-6}	7.80×10^{-7}	−96.7	12,070	$5.4\times10^{-18}\pm1.5\times10^{-18}$	$1.6\times10^{-17}\pm4.5\times10^{-18}$	$9.7\times10^{-18}\pm2.8\times10^{-18}$
Anth90-A	90	1.09	7.80×10^{-4}	5.92×10^{-4}	9.55×10^{-5}	−101.9	7610	$3.0\times10^{-15}\pm7.7\times10^{-16}$	$3.1\times10^{-15}\pm8.0\times10^{-16}$	$2.9\times10^{-15}\pm7.4\times10^{-16}$
Anth90-B	90	1.93	2.46×10^{-4}	1.71×10^{-4}	2.82×10^{-5}	−94.2	10,750	$6.7\times10^{-16}\pm1.9\times10^{-16}$	$6.4\times10^{-16}\pm1.8\times10^{-16}$	$6.0\times10^{-16}\pm1.7\times10^{-16}$
Anth90-C	90	2.99	3.70×10^{-5}	2.71×10^{-5}	4.04×10^{-6}	−89.0	13,000	$1.9\times10^{-16}\pm4.9\times10^{-17}$	$1.9\times10^{-16}\pm5.0\times10^{-17}$	$1.6\times10^{-16}\pm4.2\times10^{-17}$
Anth90-D	90	3.55	1.34×10^{-5}	9.85×10^{-6}	1.70×10^{-6}	−86.8	12,940	$7.2\times10^{-17}\pm1.8\times10^{-17}$	$7.3\times10^{-17}\pm1.9\times10^{-17}$	$7.2\times10^{-17}\pm1.8\times10^{-17}$

[a]At experimental temperature.
[b]Initial specific surface area = 12,100 cm^2 g^{-1}.
[c]Rates are in mol anthophyllite, using the analyzed composition listed in Table 1.

Eq. (5) vary from −44 to −29 kcal mol^{-1}, and for anthophyllite calculated based on Eq. (6) vary from −130 to −87 kcal mol^{-1} (Table 4).

4. Discussion

4.1. Dissolution rates of diopside and anthophyllite

Comparison of dissolution rates obtained from this study with data from the literature shows that our dissolution rates at 25°C for diopside and anthophyllite are lower than those estimated by other workers for the same phases under similar pH and temperature conditions (Schott et al., 1981; Eggleston et al., 1989; Knauss et al., 1993). The observed discrepancy may be related to factors such as run duration, use of buffers, change in surface area, and differences in the materials used. If we assume that for most of the silicates, the initial fast transient dissolution period is followed by a slow approach to steady state, then the rates obtained from our long duration experiments are probably closer to the true steady state dissolution rates than those obtained from short experiments [Schott et al. (1981), 2–40 days]. Also, while most of the other workers used buffer solutions in their experiments, no buffers were used in our experiments, thus eliminating the possibility of promoting or inhibiting the dissolution rates. In addition, most previous workers normalized the dissolution rates using the initial surface area while in this work we used final surface area, which is up to a factor of 3 higher than the initial area. However, comparison of previously reported rates with our rates shows that the literature rates are higher than ours, even if corrections are made for surface area differences or run durations. Therefore, differences in starting materials and reactant solutions is presumed to dominate discrepancies.

4.2. Change in surface area

Tables 3 and 4 demonstrate that depending on temperature and pH, after the experiments, the specific surface area of diopside ranged from unchanged (e.g., Run Diop25-1, from 860 to 880 $cm^2\ g^{-1}$) to increased by factors as large as 2.7 (e.g., Run Diop90-C, from 860 to 2340 $cm^2\ g^{-1}$). It is expected that the observed increase in surface area of diopside is caused by the increase in surface roughness which results from preferential dissolution of exsolution lamellae, dissolution at dislocations, or at other imperfect sites on the surface of the mineral. Fig. 3A is a scanning electron photomicrograph (SEM) of diopside before experiment. Increase in surface roughness was observed on a few reacted samples as shown on Fig. 3B (leached at 90°C and pH 3.18). The microtopography observed on the sample imaged in Fig. 3B is probably developed along the exsolution lamellae boundaries as observed on some diopside grains under back-scattered electron microscopy (BSEM, Fig. 3C).

On the other hand, the specific surface area of fibrous anthophyllite does not change significantly after experiments. The small change in surface area of anthophyllite can be explained as the balance between loss and creation of surface area. As mentioned in the section on sample preparation, a large number of ultrafine particles were present in the starting material (Fig. 3D). After experiments, however, these ultrafine particles were absent and the anthophyllite fibers appeared clean (Fig. 3E). During the dissolution experiment, a decrease in surface area due to dissolution of ultrafines may have been compensated by the increase in new surface area due to dissolution at dislocations and other imperfect surface sites, or further break-down of the fibrous material. However, etch pits were not observed on the leached anthophyllite surface. Interestingly, a de-

Fig. 2. (a) Change of diopside dissolution rate with time at 25°C. Dissolution rate is expressed as log mol diopside ($Ca_{0.8}Mg_{0.8}Fe_{0.2}Al_{0.1}Si_2O_6$) release per cm^2 per second. Note that during the course of experiments, we doubled the flow rate. The change in flow rate is reflected by the discontinuity at about 2000 h. (b) Change of diopside dissolution rate with time at 90°C. Dissolution rate is expressed as log mol diopside ($Ca_{0.8}Mg_{0.8}Fe_{0.2}Al_{0.1}Si_2O_6$) release per cm^2 per second. (c) Change of anthophyllite dissolution rate with time at 25°C. Dissolution rate is expressed as log mol anthophyllite ($Mg_{5.7}Fe_{1.0}Al_{0.1}Si_{7.8}O_{22}(OH)_2$) release per cm^2 per second. Note that during the course of experiments, we doubled the flow rate. The change in flow rate is reflected by the discontinuity at about 2000 h. (d) Change of anthophyllite dissolution rate with time at 90°C. Dissolution rate is expressed as log mol anthophyllite ($Mg_{5.7}Fe_{1.0}Al_{0.1}Si_{7.8}O_{22}(OH)_2$) release per cm^2 per second.

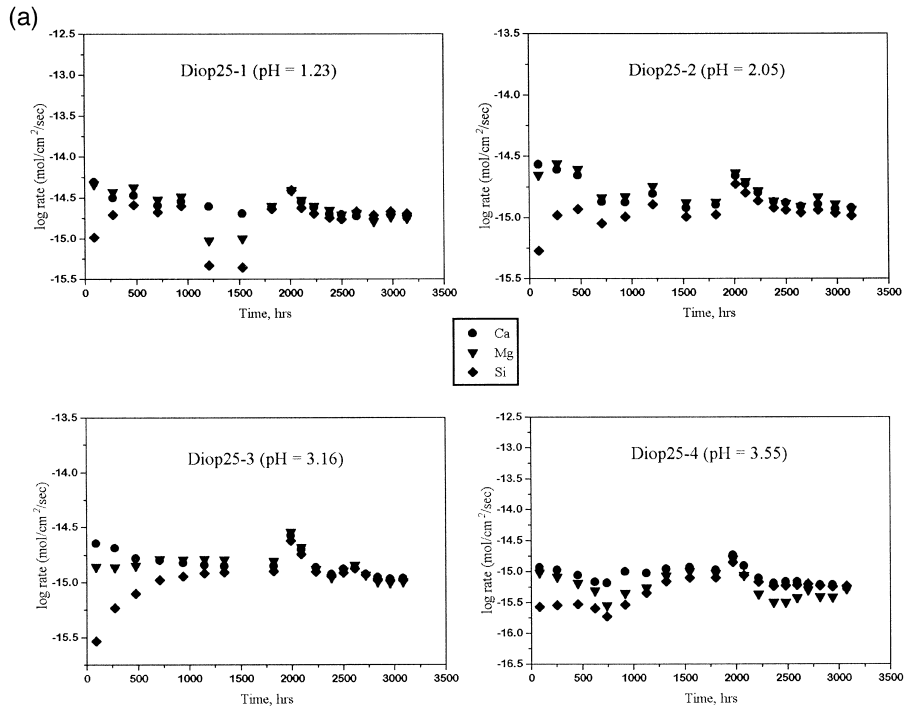
(a)
Diop25-1 (pH = 1.23)
Diop25-2 (pH = 2.05)
Diop25-3 (pH = 3.16)
Diop25-4 (pH = 3.55)
log rate (mol/cm²/sec)
Time, hrs
Ca
Mg
Si

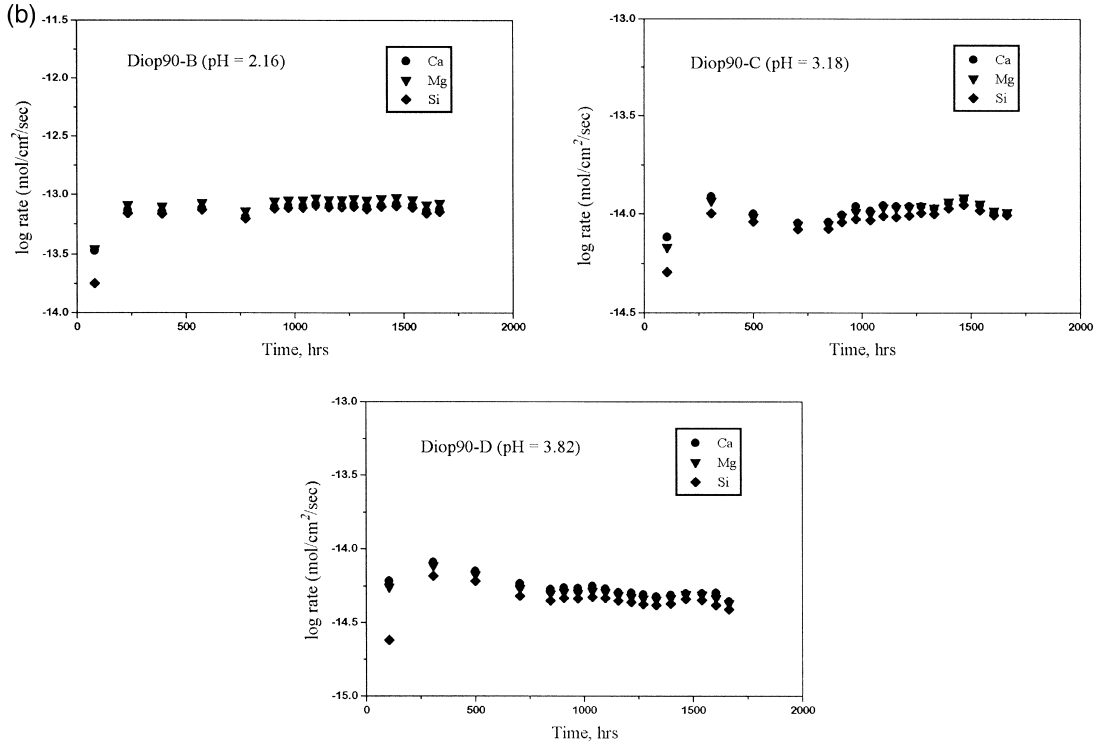
(b)
Diop90-B (pH = 2.16)
Diop90-C (pH = 3.18)
Diop90-D (pH = 3.82)
log rate (mol/cm²/sec)
Time, hrs
Ca
Mg
Si

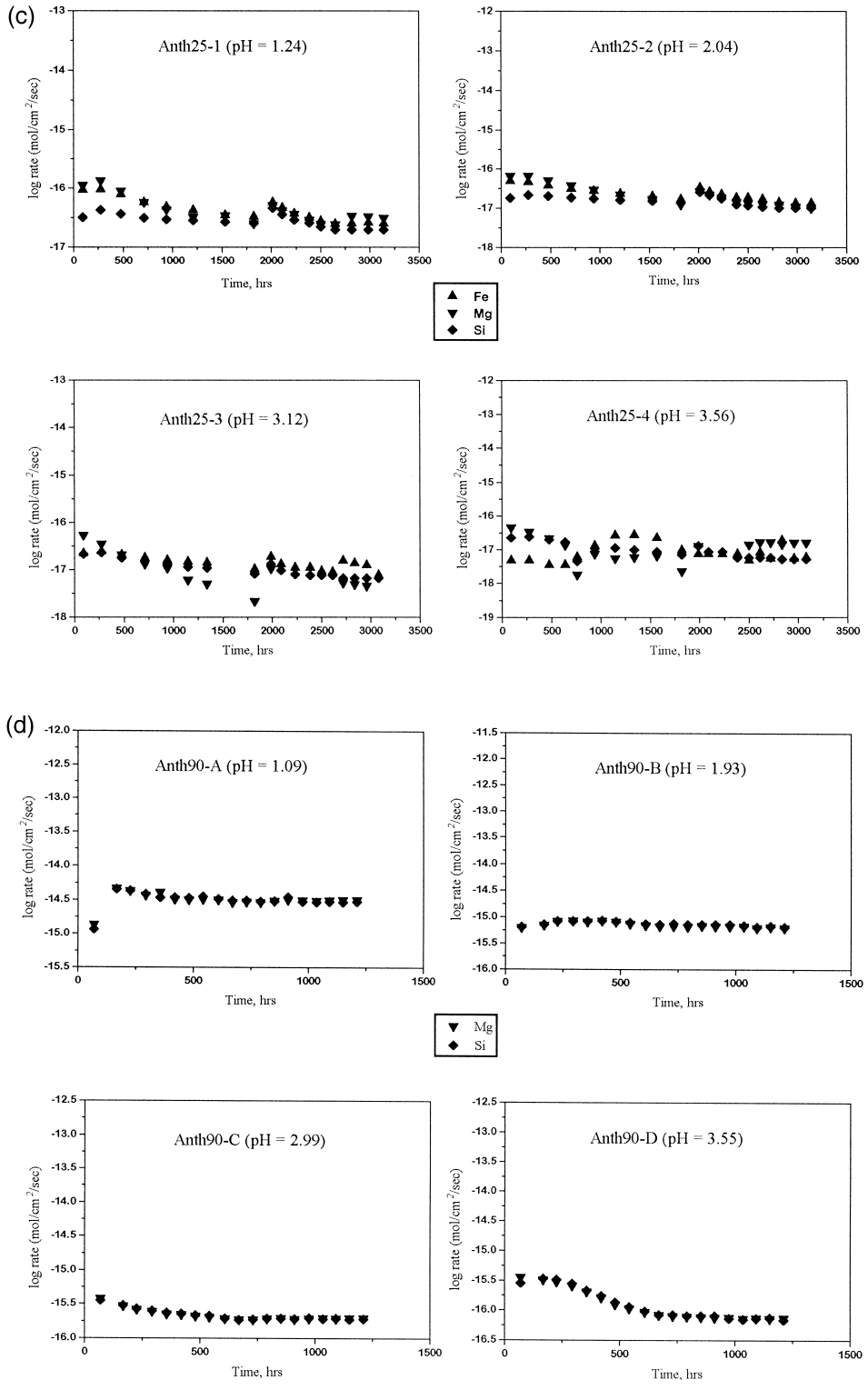

Fig. 2 (continued).

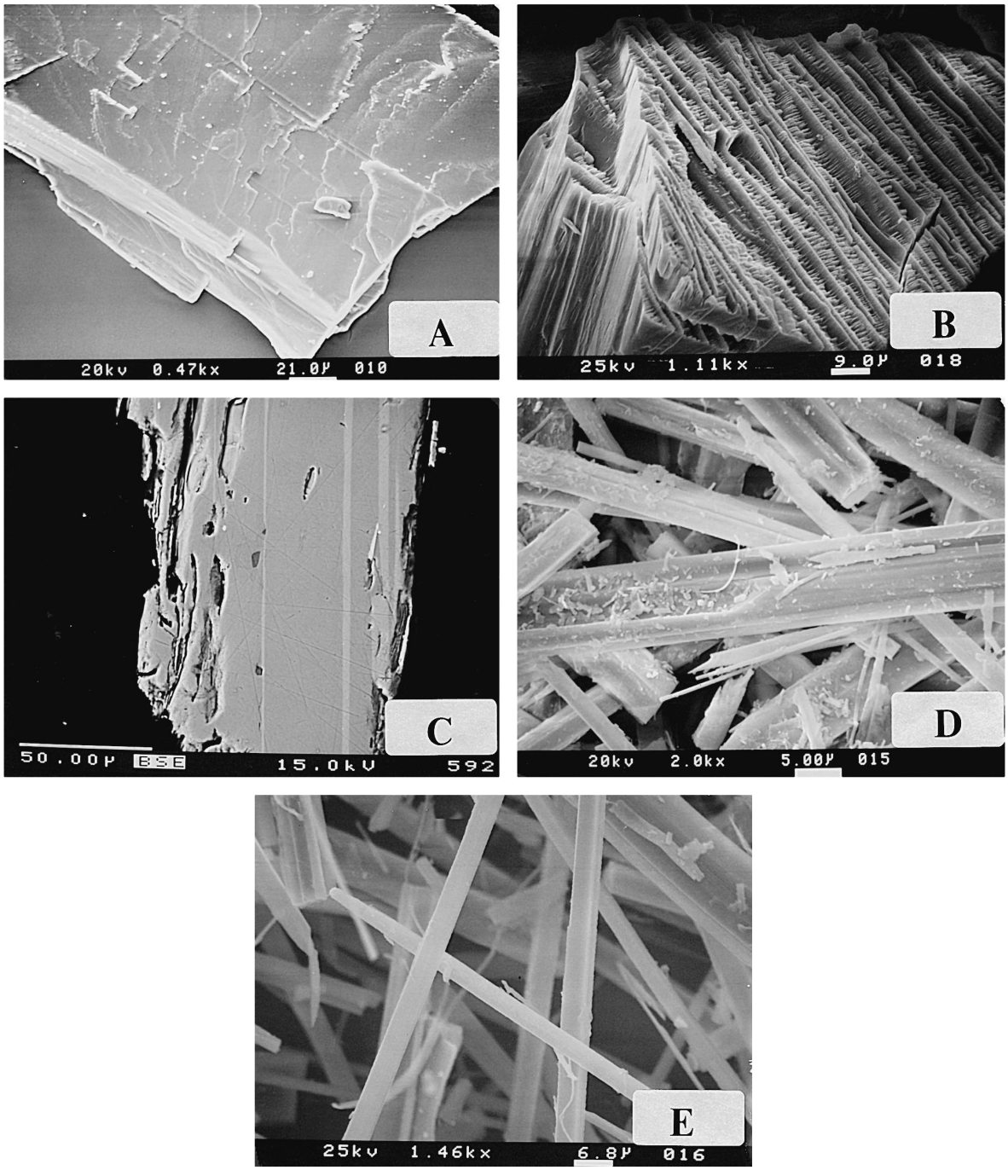

Fig. 3. (A) SEM photomicrograph showing an unleached diopside grain. (B) SEM photomicrograph showing a diopside grain leached at 90°C and pH 2.17 for 1830 h. (C) BSEM photomicrograph showing a diopside grain with exsolution lamellae. The composition of the lamellae is presented in Table 1. (D) SEM photomicrograph showing unleached anthophyllite. Many ultrafine particles are attached on the surface. (E) SEM photomicrograph showing anthophyllite leached at 90°C and pH 2.99 for 1380 h.

crease in surface area by 40% was observed for experiment at 90°C and pH 1.07 (Run Anth90-A), which may represent dissolution of ultrafines. The surface features of all leached anthophyllite reacted under various experimental conditions in this study are similar to that shown on Fig. 3E.

4.3. Etch pit formation and exsolution

Previous studies show that textural features such as etch pits can reflect the dissolution mechanisms of minerals (Berner and Holdren, 1977; Berner et al., 1980; Lasaga, 1983; Brantley et al., 1986). It is widely accepted that a pitted surface indicates a surface-reaction controlled mechanism, while a smooth, rounded surface is the result of diffusion-controlled dissolution. Examination of reacted diopside grains under SEM showed no significant change in surface feature on most of the reacted samples. However, extensively distributed etch pits were observed on some of the reacted surfaces of diopside grains (e.g., Fig. 3B). The observed etch pits are preferentially developed along the exsolution lamellar boundaries between bulk diopside and Mg, Fe-rich lamellae. The surface morphology observed on our laboratory-leached samples is very similar to that observed on naturally weathered pyroxene grains (Berner et al., 1980) which show formation of extensive etch pits along lamellae boundaries, or parallel to the *c*-axis of the crystal. Based on the observation of etch pits on the surface of weathered pyroxenes, Berner et al. (1980) concluded that weathering of these minerals is surface-reaction controlled.

By contrast, no etch pits are observed on the surfaces of leached anthophyllite. The reason for the lack of etch pits is probably related to the fibrous nature of this mineral. Preferential dissolution along the c axis would disintegrate an anthophyllite fiber into two smaller fibers, instead of creating etch pits. However, decrease in particle size of anthophyllite fibers could not be observed under SEM due to the presence of the wide range of particle sizes (35–400 mesh).

4.4. Dissolution stoichiometry

Based upon the analysis of Fig. 2A–D, steady state dissolution was reached at 2700 h (at 25°C) or 1000 h (at 90°C) for these minerals. It was also found that inosilicate dissolution stoichiometry is dependent on the rate and stage of the dissolution reaction. At 25°C, dissolution of both diopside and anthophyllite appeared non-stoichiometric at the early stages of the reaction, and became more stoichiometric with time. For most experiments, the initial release rates of alkaline earth elements were faster than those for Si, although there are some uncertainties in determining the relative release rates of Mg and Si for anthophyllite dissolution at $pH > 3.5$, when the concentrations of these elements were very low.

The observed early stage of non-stoichiometric dissolution of inosilicates at acidic pH is in agreement with reports by other workers (Luce et al., 1972; Sanemasa and Kataura, 1973; Grandstaff, 1977; Schott et al., 1981; Schott and Berner, 1983, 1985; Knauss et al., 1993). Hoch et al. (1995) found that dissolution of augite was non-stoichiometric even after 1.5 years in a flow-through reactor. Some workers also reported that cations in the M2 site of pyroxene were released more rapidly than those in the M1 site [e.g., Ca released faster than Mg in diopside, see the works of Sanemasa and Kataura (1973) and Schott et al. (1981)] and that cations in the M4 site were released faster than those in the M1, M2, or M3 sites in amphibole [e.g., Ca released faster than Mg in hornblende, see the works of Barman et al. (1992) and Zhang et al. (1993)]. However, the preferential release of Ca over Mg from diopside is not as clearly shown in our experiments.

At 90°C, dissolution of diopside and anthophyllite was more nearly stoichiometric than dissolution at 25°C. During all dissolution experiments of anthophyllite at 90°C, dissolution was stoichiometric (Fig. 2B and D).

4.5. pH-dependence

The log (dissolution rates) of diopside and anthophyllite are plotted in Fig. 4A and B vs. pH for experiments at temperatures of 25° and 90°C. These plots show a good linear relationship between log rate and pH. Values of n, as defined in Eq. (1), have been calculated using linear regression and summarized in Table 5.

Our estimated value of n for diopside dissolution at 25°C is similar to that estimated by Knauss et al. (1993) ($n \approx 0.2$). However, unlike their report, in which they observed that n remained constant at

temperatures between 25° and 70°C, we observed an almost four-fold increase in the value of n when temperature increased to 90°C. One source of the discrepancy may be that in their experiments, buffer solutions were used to keep the pH constant, while in our experiments, only $HCl + H_2O$ were used. As proposed by Dove and Crerar (1990) for quartz, the use of buffer solutions may cause inhibition or acceleration of dissolution. The higher values of n for diopside dissolution in our 90°C experiments are similar to those reported by Schott et al. (1981) and Schott and Berner (1985) for the same phase ($n = 0.75$ at 50°C), although these authors used buffers in their experiments. Discrepancies among the data reported by different researchers suggest that in addition to buffers, other factors may also affect the rate of dissolution.

Unlike Mast and Drever (1987), who found no pH-dependence for the dissolution rate of anthophyllite between pH 1 and 5 at 22°C [Note: rate at pH 1 in their paper was taken from the work of Schott et al. (1981)], we observed a significant pH-dependence at 25°. The difference in reaction time may contribute to the discrepancy among the results: each of our experiments ran for 3400 h, while most of the experiments of Mast and Drever (1987) ran for only ~ 100 h at a given pH. A true steady state might not have been obtained in their experiments.

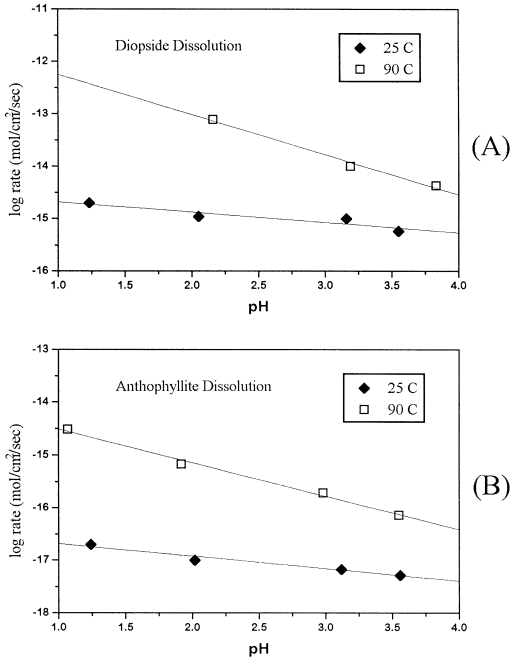

Fig. 4. pH-dependence of dissolution rate (mol diopside or anthophyllite cm^{-2} s^{-1}) at 25° and 90°C for (A) diopside, and (B) anthophyllite.

Table 5
Reaction order and activation energy

	n[a]	E_a[b] (kcal mol^{-1})
Diopside	0.19 ± 0.06 (25°C)	22.8 ± 1.6
	0.76 ± 0.08 (90°C)	
Anthophyllite	0.24 ± 0.03 (25°C)	19.4 ± 0.9
	0.63 ± 0.04 (90°C)	

[a]Reaction order with respect to H^+ defined in Eq. (1); error estimates were based on standard deviation.
[b]Activation energy defined in Eq. (8); error estimates were based on standard deviation.

It is interesting to note that if the data from our anthophyllite dissolution experiments at 25°C at approximately 100 h (see Fig. 2C) are used, the Si release rate would be independent of pH, just as observed by Mast and Drever (1987).

Like diopside dissolution, the value of n for anthophyllite dissolution was observed to increase with increase in temperature. However, the magnitude of increase in n is much smaller for anthophyllite than for diopside.

The increase in pH-dependence at higher temperature, as observed in this study, is in agreement with the conclusions of the surface protonation model, and the conclusions derived by Brady and Walther (1992) and Casey and Sposito (1992). In the Casey and Sposito model, under the condition of $pH \ll pH_{pznpc}$, the activation energy of dissolution consists of three contributions: a term reflecting the change in rate constant with respect to temperature, a term related to standard proton adsorption enthalpy, and a term related to surface potential. According to the authors, contribution from the third term is of correct magnitude and sign to produce the increased activation energies observed for mineral dissolution far from equilibrium at $pH \ll pH_{pznpc}$. The value of pH_{pznpc} for diopside has been estimated to be 7.25 (Parks, 1967) or 7.3 (Sverjensky, 1994), and the value of pH_{pznpc} for anthophyllite is estimated as 6.79 (Parks, 1967) or 6.6 (Sverjensky, 1994). Therefore, our observations are in agreement with model predictions of an increased pH-dependence with tem-

perature for diopside and anthophyllite dissolution for $pH < pH_{pznpc}$.

4.6. Activation energy of reaction

There are two 'types' of activation energy of reaction reported in the literature for silicate dissolution: pH-dependent E_a' and pH-independent E_a. The pH-dependent activation energy E_a' has typically been estimated using the following modified Arrhenius equation:

$$\ln(r_1/r_2) = (E_a'/R)(1/T_2 - 1/T_1) \quad (7)$$

where r_1 and r_2 are the dissolution rates at the pH of interest at temperatures T_1 and T_2, respectively. Using this equation, it is apparent that E_a' will be a function of pH if the value of n defined in Eq. (1) varies as a function of temperature.

The pH-independent activation energy, E_a, is calculated using the traditional Arrhenius equation:

$$\ln(k_1/k_2) = (E_a/R)(1/T_2 - 1/T_1) \quad (8)$$

where k_1 and k_2 are the rate constants determined at T_1 and T_2 respectively. Obviously, as k_1 and k_2 are independent of pH, E_a is pH-independent, too. If we compare Eqs. (7), (8) and (2), it is clear that the pH-independent activation energy can be conceptualized as a special case of the pH-dependent activation energy for pH = 0.

The values of E_a' have been calculated using Eq. (7) and the estimated dissolution rates using linear interpolation. The plots of E_a' vs. pH are shown in Fig. 5A for diopside and Fig. 5B for anthophyllite. The pH-dependent activation energy becomes very small at pH 4, approaching the value estimated for transport control (Lasaga, 1984). The pH-independent E_a values are reported in Table 5: 22.8 kcal mol^{-1} for diopside and 19.4 kcal mol^{-1} for anthophyllite. Both values are well above the E_a of transport in solution (5 kcal mol^{-1}), and significantly smaller than the E_a of breaking bonds in crystals, and are consistent with surface-controlled dissolution (Lasaga, 1984).

Although the value of E_a is large for diopside and anthophyllite, in agreement with the conclusions of Brady and Carroll (1994), this large activation energy may not be appropriate for use in describing silicate dissolution in long-term carbon cycle models. For most climate change models, pH-dependence is ignored; therefore, silicate dissolution in such a model

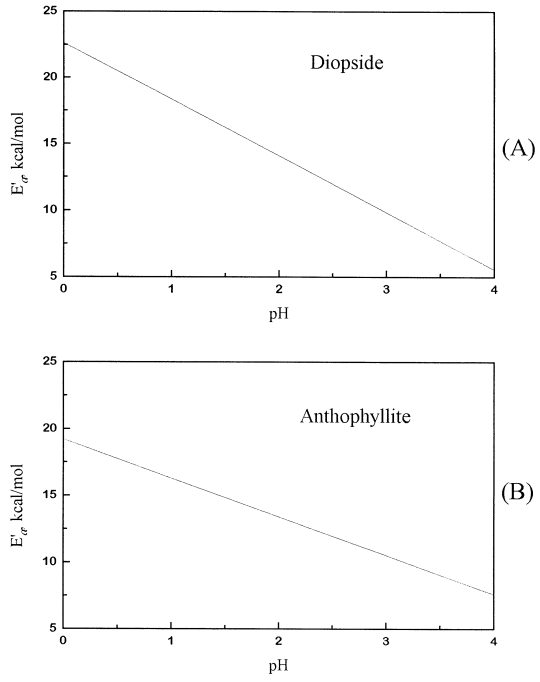

Fig. 5. pH-dependence of apparent activation energies of dissolution of (A) diopside, and (B) anthophyllite. Activation energies were calculated using Eq. (7) and the estimated dissolution rates using linear interpolation.

should be described using an activation energy for a generalized soil porewater pH—i.e., $4 < pH < \sim 7$. Under those conditions, Fig. 5A and B show that the appropriate activation energy should be quite small. The exact values of E_a, however, cannot be estimated from this study. Decrease in E_a with respect to pH is expected to be non-linear at pH > 4.

5. Conclusions

Results of diopside and anthophyllite dissolution experiments at temperatures of 25° and 90°C and acid pH show that steady state dissolution was reached after 2700 (at 25°C) to 1000 h (at 90°C). In most cases, stoichiometric dissolution was obtained; however, low concentrations made it difficult to determine all elemental concentrations with equal certainty. Depending on temperature and pH, after the experiments, the specific surface area of diopside increased by factors up to 2.7, while the specific surface area of fibrous anthophyllite did not change significantly, or decreased. Increase in surface area

of diopside samples is caused by increase in surface roughness, as observed from the SEM photos. Preferential dissolution of ultrafines attached to the surface of fibrous anthophyllite has been observed on SEM photomicrographs. It is assumed that loss of specific surface area was due to dissolution of ultrafines, and that this loss in other cases was compensated by an increase in numbers of anthophyllite fibers.

Examination of samples under SEM shows that deeply striated surfaces are formed on some of the reacted diopside grains. The observed parallelism of striations on laboratory leached diopside is very similar to that observed on naturally weathered samples of the same mineral by other workers. In contrast to diopside, no etching is found on the dissolved surfaces of anthophyllite.

A good linear relationship is observed between log dissolution rate and solution pH for anthophyllite as well as for diopside. The n values defining the pH-dependence of dissolution rate are 0.19 ± 0.06 at 25°C and 0.76 ± 0.08 at 90°C for diopside and 0.24 ± 0.03 at 25°C and 0.63 ± 0.04 at 90°C for anthophyllite. The pH dependence increases with increasing temperature, and the rate of increase is greater for diopside than for anthophyllite.

Activation energies have been estimated for diopside and anthophyllite dissolution. The values of pH-independent activation energies are 22.8 ± 1.6 and 19.4 ± 0.9 kcal mol^{-1} for diopside and anthophyllite, respectively. Both values are well above E_a of transport in solution (5 kcal mol^{-1}), and significantly smaller than the E_a of breaking bonds in crystals (Lasaga, 1984).

It is also found that the temperature-dependence of the dissolution rate of diopside and anthophyllite are strongly pH-dependent. Therefore, modeling of the long-term dissolution rates of Ca, Mg-containing minerals for global climate models should incorporate the activation energy appropriate for the pH of interest. These apparent activation energies tend to be smaller than the pH-independent activation energy defined by Eq. (1) and the Arrhenius equation.

Acknowledgements

The authors thank Drs. J. Drever, K. Knauss and P. Maurice for their technical reviews of this manuscript. Special appreciation is also due to Dr. A. Rose, Mr. D. Voigt and Mrs. C. Perry of the Pennsylvania State University for helpful discussions and assistance. This research was funded through grants from the National Science Foundation (EAR 9305141 and EAR 8657868), and from the David and Lucile Packard Foundation, to S.L.B. The first author would also like to thank the Department of Geosciences, the Pennsylvania State University, for providing Krynine Scholarship to present research at scientific meetings.

References

Banfield, J.F., Ferruzzi, C.G., Casey, W.H., Westrich, H.R., 1995. HRTEM study comparing naturally and experimentally weathered pyroxenoids. Geochim. Cosmochim. Acta 59, 19–31.

Barman, A.K., Varadachari, C., Ghosh, K., 1992. Weathering of silicate minerals by organic acids: I. Nature of cation solubilisation. Geoderma 53, 45–63.

Berner, R.A., Holdren, G.R., 1977. Mechanism of feldspar weathering: some observational evidence. Geology (Bolder) 5, 369–372.

Berner, R.A., Sjoberg, E.L., Velbel, M.A., Krom, M.D., 1980. Dissolution of pyroxenes and amphiboles during weathering. Science 207, 1205–1206.

Blum, A.E., Lasaga, A.C., 1988. Role of surface speciation in the low-temperature dissolution of minerals. Nature 331, 431–433.

Blum, A.E., Lasaga, A.C., 1991. The role of surface speciation in the dissolution of albite. Geochim. Cosmochim. Acta 55, 2193–2201.

Brady, P.V., Carroll, S.A., 1994. Direct effects of CO_2 and temperature on silicate weathering: possible implications for climate control. Geochim. Cosmochim. Acta 58, 1853–1856.

Brady, P.V., Walther, J.V., 1989. Controls on silicate dissolution rates in natural and basic pH solutions at 25 degrees C. Geochim. Cosmochim. Acta 53, 2823–2830.

Brady, P.V., Walther, J.V., 1992. Surface chemistry and silicate dissolution at elevated temperature. Am. J. Sci. 292, 639–658.

Brantley, S.L., Chen, Y., 1995. Chemical weathering rates of pyroxenes and amphiboles. In: White, A.F., Brantley, S.L. (Eds.), Chemical Weathering Rates of Silicate Minerals. Reviews in Mineralogy, 31, pp. 119–172.

Brantley, S.L., Crane, S.R., Crerar, D.A., Hellmann, R., Stallard, R., 1986. Dissolution at dislocation etch pits in quartz. Geochim. Cosmochim. Acta 50, 2349–2361.

Casey, W.H., Sposito, G., 1992. On the temperature dependence of mineral dissolution rates. Geochim. Cosmochim. Acta 56, 3825–3830.

Chen, Y., Brantley, S.L., 1997. Temperature- and pH-dependence of albite dissolution rate at acid pH. Chem. Geol. 135, 275–290.

Dove, P.M., Crerar, D.A., 1990. Kinetics of quartz dissolution in electrolyte solutions using a hydrothermal mixed flow reactor. Geochim. Cosmochim. Acta 54, 955–969.

Drever, J.I., Murphy, K.M., Clow, D.W., 1994. Field weathering rates versus laboratory dissolution rates: an update. Mineral. Mag. 58A, 239–240.

Eggleston, C.M., Hochella, M.F., Parks, G.A., 1989. Sample preparation and aging effects on the dissolution rate and surface composition of diopside. Geochim. Cosmochim. Acta 53, 797–804.

Ferruzzi, G.G., 1993. The character and rates of dissolution of pyroxenes and pyroxenoids. MS thesis, Univ. California, Davis, CA.

Grandstaff, D.E., 1977. Some kinetics of bronzite orthopyroxene dissolution. Geochim. Cosmochim. Acta 41, 1097–1103.

Greenberg, A.E., Trussell, P.R., Clesceri, L.S. (Eds.), 1985. Standard methods for the examination of water and wastewater. Am. Public Health Ass., Washington DC, pp. 460–461.

Helgeson, H.C., 1985. SUPCRT—unpublished thermodynamic data base for minerals, aqueous species and gases. Univ. of California, Berkeley, CA.

Helgeson, H.C., Delany, J.M., Nesbitt, H.W., Bird, D.K., 1978. Summary and critique of the thermodynamic properties of rock-forming minerals. Am. J. Sci. 278A, 229.

Hill, C.G., 1977. An Introduction to Chemical Engineering Kinetics and Reactor Design. Wiley, New York, 594 pp.

Hoch, A.R., Claassen, H.C., Drever, J.I., Reddy, M.M., 1995. Dissolution stoichiometry and near-surface mineral chemistry of augite after 1.5 years in a flow-through reactor, with implications for reaction mechanism and watershed-scale mass balance calculations. Geol. Sco. Am. Abstr. Programs 27 (6), A–184.

Kharaka, Y.K., Gunter, W.D., Aggarwal, P.K., Perkins, E.H., DeBraal, J.D., 1988. SOLMIN88: a computer program for geochemical modeling of water–rock interaction. USGS Water-Resources Invest. Report 88-4227.

Knauss, K.G., Nguyen, S.N., Weed, H.C., 1993. Diopside dissolution kinetics as a function of pH, CO_2, temperature, and time. Geochim. Cosmochim. Acta 57, 285–294.

Laidler, K.J., 1987. Chemical Kinetics, 3rd edn. Harper and Row, New York.

Lasaga, A.C., 1983. Kinetics of silicate dissolution. Fourth International Symposium on Water–Rock Interaction, pp. 269–274.

Lasaga, A.C., 1984. Chemical kinetics of water–rock interactions. J. Geophys. Res. 89, 4009–4025.

Luce, R.W., Bartlett, R.W., Parks, G.A., 1972. Dissolution kinetics of magnesium silicates. Geochim. Cosmochim. Acta 36, 35–50.

Machesky, M.L., 1989. Influence of temperature on ion adsorption by hydrous metal oxides. In: Melchior, D.C., Bassett, R.L. (Eds.), Chemical Modeling of Aqueous System: II. American Chemical Society. ACS Symposium Series, 416, pp. 282–292.

Mast, M.A., Drever, J.I., 1987. The effect of oxalate on the dissolution rates of oligoclase and tremolite. Geochim. Cosmochim. Acta 51, 2559–2568.

Murphy, K.M., Drever, J.I., 1993. Dissolution rate of albite as a function of grain size. American Geophysical Union Spring Meeting, EOS Supplement, p. 329.

Parks, G.A., 1967. Aqueous surface chemistry of oxides and complex oxide minerals. Equilibrium Concepts in Natural Water Systems. American Chemical Society Adv. Chemistry Series, 67, pp. 121–160.

Rimstidt, J.D., Dove, P.M., 1986. Mineral/solution reaction rates in a mixed flow reactor: wollastonite hydrolysis. Geochim. Cosmochim. Acta 50, 2509–2516.

Robie, R.A., Hemingway, B.S., Fisher, J.R., 1978. Thermodynamic properties of minerals and related substances at 298.15 K and 1 bar pressure and at higher pressures. USGS Bull. 1452, 456.

Sanemasa, I., Kataura, T., 1973. The dissolution of $CaMg(SiO_3)_2$ in acid solutions. Bull. Chem. Soc. Jpn. 46, 3416–3422.

Schindler, P.W., 1981. Surface complexes at oxide–water interfaces. In: Anderson, M.A. (Ed.), Adsorption of Inorganics at Solid–Liquid Interfaces. Ann Arbor Sci. Publ., Ann Arbor, MI, pp. 1–150.

Schott, J., Berner, R.A., 1983. X-ray photoelectron studies of the mechanism of iron silicate dissolution during weathering. Geochim. Cosmochim. Acta 47, 2233–2240.

Schott, J., Berner, R.A., 1985. Dissolution mechanisms of pyroxenes and olivines during weathering. In: Drever, J.I. (Ed.), The Chemistry of Weathering, Vol. 149. Reidel, Dordrecht.

Schott, J., Petit, J.C., 1987. New evidence for the mechanisms of dissolution of silicate minerals. In: Stumm, W. (Ed.), Aquatic Surface Chemistry: Chemical Processes at the Particle–Water Interface. Swiss Fed. Inst. Tech., Zurich, Switzerland, pp. 293–315.

Schott, J., Berner, R.A., Sjoberg, E.L., 1981. Mechanism of pyroxene and amphibole weathering: I. Experimental studies of iron-free minerals. Geochim. Cosmochim. Acta 45, 2123–2135.

Shapiro, L., 1975. Rapid analysis of silicate, carbonate, and phosphate rocks—revised edition. USGS Bull. 1401, 76.

Siegel, D.I., Pfannkuch, H.O., 1984. Silicate mineral dissolution at pH 4 and near standard temperature and pressure. Geochim. Cosmochim. Acta 48, 197–201.

Stillings, L.L., Brantley, S.L., 1995. Feldspar dissolution at 25°C and pH 3: reaction stoichiometry and the effect of cations. Geochim. Cosmochim. Acta 59, 1483–1496.

Stumm, W., Furrer, G., 1987. The dissolution of oxides and aluminum silicates: examples of surface-coordination-controlled kinetics. In: Stumm, W. (Ed.), Aquatic Surface Chemistry. Wiley, New York, pp. 197–220.

Sverdrup, H.U., 1990. The Kinetics of Base Cation Release Due to Chemical Weathering. Lund Univ. Press.

Sverjensky, D.A., 1994. Zero-point-of-charge prediction from crystal chemistry and solvation theory. Geochim. Cosmochim. Acta 58, 3123–3129.

Xie, Z., 1994. Surface properties of silicates, their solubility and dissolution kinetics. PhD dissertation, Northwestern Univ., Evanston, IL.

Xie, Z., Walther, J.V., 1994. Dissolution stoichiometry and adsorption of alkali and alkaline earth elements to the acid-reacted wollastonite surface at 25 degrees C. Geochim. Cosmochim. Acta 58, 2587–2598.

Zhang, H., Bloom, P.R., Nater, E.A., 1993. Change in surface area and dissolution rates during hornblende dissolution at pH 4.0. Geochim. Cosmochim. Acta 57, 1681–1689.